ChemComm

COMMUNICATION

View Article Online
View Journal | View Issue

Cite this: *Chem. Commun.*, 2017, 53, 1751

Received 10th December 2016,
Accepted 13th January 2017

DOI: 10.1039/c6cc09832k

www.rsc.org/chemcomm

Electrospun metal–organic framework derived hierarchical carbon nanofibers with high performance for supercapacitors†

Chaohai Wang, Chao Liu, Jiansheng Li,* Xiuyun Sun, Jinyou Shen, Weiqing Han and Lianjun Wang*

A novel N-doped MOF-based hierarchical carbon fiber (NPCF) towards supercapacitors was prepared by the pyrolysis of MOF nanofibers. Due to its unique 1D hollow structures, the NPCF exhibits better energy storage capacity than the other previously reported MOF-derived carbon materials.

Supercapacitors (SCs), also called electrochemical capacitors, have drawn great attention because of their high power density, rapid charging–discharging capacity and long cyclic life in the past few years.[1–3] Carbon materials, especially nanoporous carbons (NPCs), are the most widely used materials for SCs, due to their many advantages, including high surface area, easy processing, non-toxicity and good electronic conductivity.[4,5] To date, a variety methods have been developed for the preparation of NPCs, such as, direct carbonization of organic precursors,[6] electrical arc,[7] templating[8] and CVD (chemical vapor decomposition) methods, *etc.*[9] Among them, based on its flexibility and simplicity, direct pyrolysis is the most common way to synthesize NPCs. However, the NPC obtained through this method often contains various sizes, disordered structures and low surfaces, which greatly limit their applications.[10] Therefore, how to get NPCs with ordered pore structures and relatively uniform pore sizes has become a hot research area.

Recently, metal–organic frameworks (MOFs), as a new class of precursors to synthesize carbon materials (MOF-C), have attracted much attention.[11,12] Compared with traditional organic precursors, MOFs have ordered structures, higher surface areas and inherent presence of heteroatoms, which are highly desirable for SC performance.[13] On the other hand, when directly using MOFs as precursors for the synthesis of NPCs, the resulting MOF-C can retain the initial features of the parent MOFs. In 2008, Xu *et al.* first reported the MOF-derived NPC with high surface area and used for electrochemical double-layered capacitors (EDLCs).[14] After that, many groups carried out the relevant research work and have achieved many results.[15–20] However, due to the intrinsic nature of MOFs, MOF-derived NPCs have many micropores, which may influence their conductivity, resulting in the weakening of their capacitance. In addition, their poor conductivity is attributed to the lack of connection between MOF-Cs, and the specific capacitance of them is 100–300 F g^{-1} in aqueous electrolytes, having no obvious advantages compared to other carbon materials.[21a] Although MOF-derived NPCs have ordered porous structures and high surface areas, their electrical conductivity, another major prerequisite for the active materials used in the SCs, is still relatively weak. Therefore, it is still a great challenge to build high-performance SCs based on MOF-C.

Recently, Wang *et al.* reported a new method for overcoming the insulation problems of MOFs by electrochemically interweaving MOF crystals with a conductive polymer.[21b] Inspired by this strategy we demonstrated an effective way to enhance the conductivity performance of NPCs by electrospinning. Specifically, ZIF-8/PAN nanofibers were synthesized *via* electrospinning and further carbonization to 1D nanoporous carbon fibers (NCPFs) (Scheme 1), and the detailed experimental methods can be found in the ESI.† As shown in Fig. S1 (ESI†), a non-woven film

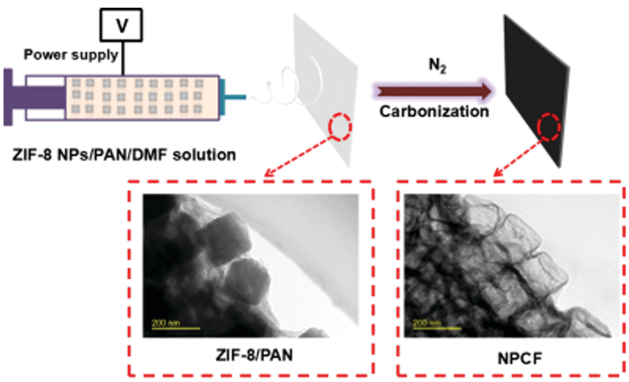

Scheme 1 Preparation process of nanoporous carbon fibers (NCPFs).

Jiangsu Key Laboratory of Chemical Pollution Control and Resources Reuse, School of Environmental and Biological Engineering, Nanjing University of Science and Technology, Nanjing 210094, People's Republic of China. E-mail: lijsh@njust.edu.cn

† Electronic supplementary information (ESI) available: Experimental details, SEM images, XRD patterns, TG data, N_2 sorption isotherms, XPS and FTIR spectra. See DOI: 10.1039/c6cc09832k

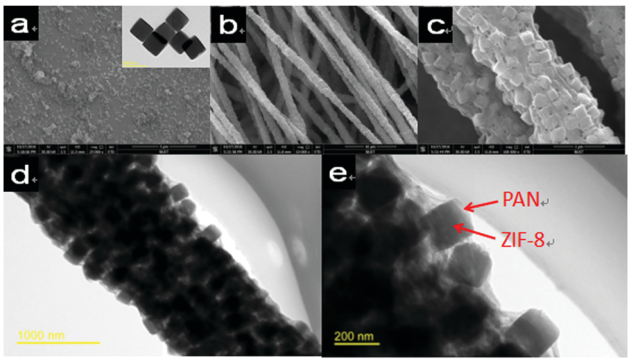

Fig. 1 (a) SEM images of ZIF-8, inset in (a) is TEM; (b and c) SEM images, (d and e) TEM images of ZIF-8/PAN.

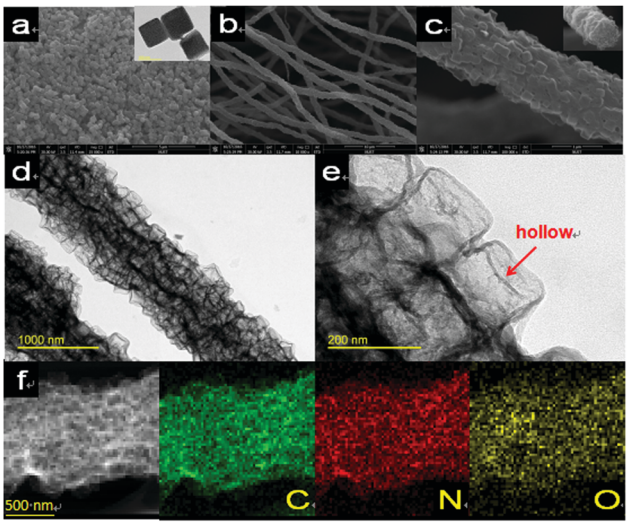

Fig. 2 (a) SEM image of ZIF-8-NPC, inset in (a) is TEM image; (b and c) SEM images of NPCF, inset of (c) is the corresponding sectional image of NPCF; (d and e) TEM images of NPCF; and (f) STEM image and corresponding element mapping of NPCF.

of ZIF-8/PAN nanofibers in white color is obtained after the electrospinning process. After heat-treatment in a N_2 atmosphere, the white precursor film is transformed into a black film.

SEM and TEM images of the ZIF-8 nanoparticles and ZIF-8/PAN are fully demonstrated in Fig. 1, and PAN fibers in Fig. S3a (ESI†). As shown in Fig. 1a, the as-synthesized ZIF-8 nanoparticles are uniform in size (around 200 nm). And the TEM image reveals that the dispersity of ZIF-8 nanoparticles is good, which is important for electrospinning. The powder X-ray diffraction (XRD) patterns of synthesized ZIF-8 are consistent with the simulated spectra, suggesting that the purity and crystallinity of them are very high (Fig. S2a, ESI†). By electrospinning, the ZIF-8/PAN/DMF solution was converted into continuous ZIF-8/PAN fibers. The length of the fibers can reach the millimeter or even centimeter grade with a diameter of $\sim$1.4 μm (Fig. 1b). The enlarged SEM image (Fig. 2c) shows that the ZIF-8 cubic nanocrystals coated in the PAN fibers. From the TEM image of ZIF-8/PAN (Fig. 1d), ZIF-8 nanoparticles in the interior of the nanofibrous framework were observed, indicting that the nanoparticles were distributed in the whole fiber. In a magnified TEM image (Fig. 1e), it can be seen that ZIF-8 cubic nanocrystals are evenly distributed and coated by PAN. In addition, the intensity of ZIF-8/PAN XRD patterns and IR absorption peaks show the significant reduction that is comparable to that of ZIF-8, but the location has no obvious change (Fig. S2, ESI†), which further confirmed that ZIF-8 nanoparticles were encapsulated by PAN during the electrospinning process. After the heating-treatment in a N_2 atmosphere, ZIF-8-NPC, NPCF, PAN-C were obtained and their structures were studied by SEM and TEM (Fig. 2 and Fig. S3b, ESI†). The size of ZIF-8-NPC (Fig. 2a) and the diameter of NPCF were decreased to 140 nm and $\sim$1.0 μm, attributed to the macroscopic size shrinkage of them during the carbonization process. However, a closer observation of the magnified SEM image of NPCF (Fig. 2c) found that the size of ZIF-8-NPC located in the NPCF has no obvious reduction. More interestingly, compared with PAN-C (Fig. S3b, ESI†), NPCFs have many typical mesoporous structures, meaning that the hierarchical porous structure comes from the ZIF-8. And the sectional image shows that ZIF-8-NPCs located in the NPCF have a hollow structure. To clearly observe the hollow structures, TEM is employed to characterize the NPCFs. As shown in Fig. 2d–e, the uniform hollow cubic structures, which are derived from ZIF-8, can be seen easily. Furthermore, there are also many micropores which are derived from the ZIF-8 framework in the walls of mesopores, forming a novel 1D nitrogen-enriched carbon fiber with a unique hierarchical porous structure. The hierarchical porous properties can be further confirmed by nitrogen adsorption measurements at 77 K (Fig. S4, ESI†). As shown in Fig. S4b (ESI†), NPCF shows a typical type IV isotherm, indicating the existence of mesopores. The BET surface area and pore volumes of PAN-C, ZIF-8-NPC and NPCF are listed in Table S1 (ESI†).

By comparison, in the pyrolysis process, the only difference between the ZIF-8 nanoparticles and ZIF-8 nanoparticles located in the PAN fiber is that the latter were coated by a layer of PAN. Interestingly, after carbonization under the same conditions, ZIF-8-NPC still retained the solid cubic structures; however, ZIF-8-NPC located in the NPCF transformed into hollow cubic structures. These results reveal that PAN plays an important role in the decomposition process of ZIF-8, as known as the confinement effect. According to the literature,[22,23] the possible formation mechanism of the hollow structures is deduced as follows: the surface of ZIF-8 cubic structures has abundant Zn^{2+} sites that can be coordinated with –C≡N bands abundantly existing in PAN, leading to ZIF-8 encapsulated by PAN tightly. Thermogravimetry (TG) curves show that PAN almost completely transformed into PAN-C at 500 °C (Fig. S5, ESI†), meanwhile, ZIF-8 nanoparticles have no obvious decomposition. Thereby, ZIF-8 cubic structures are encapsulated by PAN-derived carbon at 500 °C. At a low pyrolysis temperature, the PAN-derived carbon still has many –C≡N bands that can form a new strong interface between the ZIF-8 surface and the PAN-derived carbon shell, which later causes ZIF-8 cubic structures decomposed with distinct shrinkage from inside to outside. As a result, uniform hollow cubic structures are successfully formed.

We further investigated the surface chemical composition and element bonding configurations of PAN-C, ZIF-8-NPC and

NPCF using X-ray photoelectron spectroscopy (XPS). The XPS spectrum reveals the existence of C, N and O elements in the above samples (Fig. S6a, ESI†), and the relative compositions of C, N, and O ware listed in Table S1 (ESI†). EDS elemental mapping shows that the uniform distribution of C, N, and O in NPCF (Fig. 2f). High-resolution N1s spectra of NPCF can be can be deconvoluted into three peaks: pyridinic-N at ≈398.4 eV, pyrrolic-N at ≈399.6 eV and oxidized-N at ≈401.4 eV, respectively (Fig. S6b, ESI†).[24] Based on the above analysis, it is known that the NPCFs possess a 1D structure with hierarchical porous structure and are nitrogen-doped, which are main prerequisites for achieving a high-performance EDLC supercapacitor.

To evaluate the electrochemical and capacitance performance of the obtained carbon materials, CV (cyclic voltammetry) and GCD (galvanostatic charge–discharge) tests were carried out at various scan rates and current densities. As shown in Fig. 3a, the CV curves of NPCF represent a regular rectangle at different scan rates ranging from 10 to 200 mV S^{-1}, indicating that the capacitive response comes from the electric double-layer capacitance. GCD studies were carried out at various applied currents (Fig. 3b); a slight "IR drop" of the discharge curve evidences the favorable conductive behaviors of the NPCF electrode. The CV and GCD curves of PAN-C and ZIF-8-NPC are shown in Fig. S7 (ESI†). The specific gravimetric and volumetric capacitance values can be calculated from the following equation:[25]

$$C = \frac{I \times \Delta t}{m \times \Delta v}$$

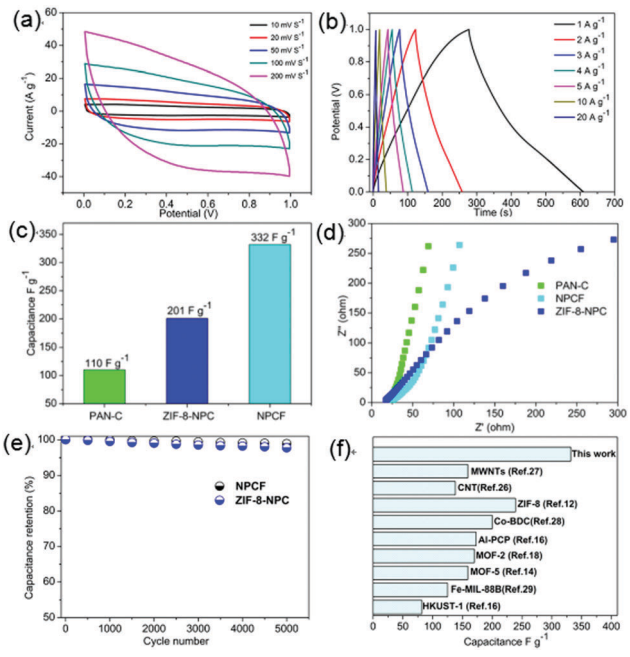

Fig. 3 (a and b) CV curves and galvanostatic charge–discharge curves of NPCF; (c) capacitance and (d) Nyquist electrochemical impedance spectra of PAN-C, ZIF-8-NPC, and NPCF; (e) cycling performance of ZIF-8-NPC and NPCF measured at 1 A g^{-1} for 5000 cycles; and (f) comparative specific capacitance with some typical MOF-derived NPC and carbon nanotubes (CNTs) and multiwall carbon nanotube (MWCNTs) in the literature.

where C (F g^{-1}) is the specific capacitance, I (A) refers to the discharge current, ΔV (V) represents the potential change within the discharge time Δt (s), and m (g) corresponds to the amount of active material on the electrode. The specific capacitances of PAN-C, ZIF-8-NPC, and NPCF were 110, 201, and 332 F g^{-1}, respectively, at 1A g^{-1} (Fig. 3c). Form Fig. 3c, it can be clearly seen that NPCF shows obvious higher specific capacitance than PAN-C and ZIF-8-PAN. The good capacitive behaviors contributed to the highly conductive NPCF. In the NPCF, the isolated ZIF-8-derived NPCs are interconnected and linked up by the chains of PAN-derived carbon that act like a "highway" to facilitate the charge transport and ionic diffusion during the electrochemical process. The Nyquist plots of PAN-C, ZIF-8-NPC, and NPCF also supported the better conductivity of NPCF over ZIF-8-NPC (Fig. 3d), and an equivalent circuit is shown in Fig. S8 (ESI†). The conductivities of ZIF-8-derived NPC, PAN-C, and NPCF were further investigated using a four-probe method. By calculation,[26] the conductivities of ZIF-8-NPC, PAN-C and NPCF were 4.32, 9.35 and 7.74 S cm^{-1}, respectively, which further confirmed that the 1D structure can improve the conductivity of ZIF-8-derived NPC. On the other hand, since ZIF-8 improves the specific surface of PAN, the capacitance of NPCF is higher than PAN-C. These results demonstrate that a synergistic effect occurs upon incorporating ZIF-8 into PAN, and the NPCF electrode benefits from the internal surface areas of ZIF-8-derived NPC and the high conductivity of PAN-C. To our knowledge, the value of 332 F g^{-1} for gravimetric and volumetric capacitance of the NPCF electrode is higher than almost all MOF-derived NPC SCs[28,29] reported to date and surpasses some other 1D carbon materials, such as carbon nanotubes (CNTs)[27a] and multiwall carbon nanotube (MWCNTs) (Fig. 3f).[27b]

Stability is another important factor for SC electrode materials in practical applications.[30] To evaluate the stability, ZIF-8-NPC and NPCF electrodes were examined using galvanostatic charge–discharge cycling at a current density of 1 A g^{-1}. As shown in Fig. 3e, after 5000 cycles, the capacity retention of NPCF is 98.9%, which is higher than that of ZIF-8-NPC (97.7%). The very high charge–discharge cyclic stability of NPCFs may be due to the following reasons: (1) NPCFs serve as numerous active units to couple with ZIF-8-NPC, which can effectively withstand large volume changes and inhibit the fusion of ZIF-8-NPC, rendering stability during the cycling process, and (2) the 1D structure provides a highly conductive nature that promotes the fast transport of electrons during the charge–discharge process.[31,32] It is noted that the chains of PAN-derived carbon not only provide efficient pathways for rapid transfer of electron charge, but also maintain structural integrity and then increase the stability of ZIF-8-derived NPCs.

To further demonstrate the structural superiority of NPCF, NPCFs with different ratios of PAN and ZIF-8 (the samples were denoted as NPCF-0.2 and NPCF-0.4) were synthesized for capacity performance tests (Fig. S9, ESI†). As shown in Fig. S10 (ESI†), with the increase of ZIF-8 content, the capacity of NPCF presented an improving trend (from 125 F g^{-1} to 332 F g^{-1}). However, when more ZIF-8 were added, the ZIF-8/PAN/DMF solution was difficult to be electrospun into fibers due to the over-high viscosity. On this basis, NPCFs-0.6 was chosen as the optimized sample.

In summary, we demonstrated a simple and effective method to enhance the supercapacitor performance of MOF-derived NPCs, by electrospinning ZIF-8 with PAN and then carbonization to N-doped MOF-based hierarchical carbon fibers. Due to their unique structures, which combine the *meso*-microporous hierarchical structure of ZIF-8-derived NPCs and the high conductivity of the carbon fiber, the value of 332 F g^{-1} for gravimetric and volumetric capacitance of the NPCF electrode is the highest among all MOF-derived NPC SCs reported to date and surpasses some other 1D carbon materials, such as carbon nanotubes (CNTs) and multiwall carbon nanotubes (MWCNTs). We believe that this work may shed light on designing new MOF-derived carbon materials for energy storage capacity and other electrochemical devices.

We would like to acknowledge the support from the National Natural Science Foundation of China (NSFC) (No. 51478224).

Notes and references

1 Y. Wang, Y. Song and Y. Xia, *Chem. Soc. Rev.*, 2016, **45**, 5925–5950.
2 S. Chen, M. Xue, Y. Li, Y. Pan, L. Zhu and S. Qiu, *J. Mater. Chem. A*, 2015, **3**, 20145–20152.
3 Y. C. Wang, W. B. Li, L. Zhao and B. Q. Xu, *Phys. Chem. Chem. Phys.*, 2016, **18**, 17941–17948.
4 J.-B. Raoof, S. R. Hosseini, R. Ojani and S. Mandegarzad, *Energy*, 2015, **90**, 1075–1081.
5 A. Mahmood, R. Zou, Q. Wang, W. Xia, H. Tabassum, B. Qiu and R. Zhao, *ACS Appl. Mater. Interfaces*, 2016, **8**, 2148–2157.
6 B. Liu, H. Shioyama, H. L. Jiang, X. B. Zhang and Q. Xu, *Carbon*, 2010, **48**, 456–463.
7 C. Journet, W. K. Maser, P. Bernier, A. Loiseau, M. L. d. L. Chapelle, S. Lefrant, P. Deniard, R. Lee and J. E. Fischer, *Nature*, 1997, **388**, 756–758.
8 F. Zhang, Y. Meng, D. Gu, Y. Yan, C. Yu, B. Tu and D. Zhao, *J. Am. Chem. Soc.*, 2005, **127**, 13508–13509.
9 B. Zheng, C. Lu, G. Gu, A. Makarovski, G. Finkelstein and J. Liu, *Nano Lett.*, 2002, **2**, 895–898.
10 J. K. Sun and Q. Xu, *Energy Environ. Sci.*, 2014, **7**, 2071–2100.
11 P. Pachfule, D. Shinde, M. Majumder and Q. Xu, *Nat. Chem.*, 2016, **8**, 718–724.
12 W. Chaikittisilp, M. Hu, H. Wang, H. S. Huang, T. Fujita, K. C. Wu, L. C. Chen, Y. Yamauchi and K. Ariga, *Chem. Commun.*, 2012, **48**, 7259–7261.
13 W. Xia, A. Mahmood, R. Zou and Q. Xu, *Energy Environ. Sci.*, 2015, **8**, 1837–1866.
14 B. Liu, H. Shioyama, T. Akita and Q. Xu, *J. Am. Chem. Soc.*, 2008, **130**, 5390–5391.
15 R. R. Salunkhe, Y. Kamachi, N. L. Torad, S. M. Hwang, Z. Sun, S. X. Dou, J. H. Kim and Y. Yamauchi, *J. Mater. Chem. A*, 2014, **2**, 19848–19854.
16 X. Yan, X. Li, Z. Yan and S. Komarneni, *Appl. Surf. Sci.*, 2014, **308**, 306–310.
17 W. Meng, W. Chen, L. Zhao, Y. Huang, M. Zhu, Y. Huang, Y. Fu, F. Geng, J. Yu, X. Chen and C. Zhi, *Nano Energy*, 2014, **8**, 133–140.
18 H. B. Aiyappa, P. Pachfule, R. Banerjee and S. Kurungot, *Cryst. Growth Des.*, 2013, **13**, 4195–4199.
19 J. W. Jeon, R. Sharma, P. Meduri, B. W. Arey, H. T. Schaef, J. L. Lutkenhaus, J. P. Lemmon, P. K. Thallapally, M. I. Nandasiri, B. P. McGrail and S. K. Nune, *ACS Appl. Mater. Interfaces*, 2014, **6**, 7214–7222.
20 F. Hao, L. Li, X. Zhang and J. Chen, *Mater. Res. Bull.*, 2015, **66**, 88–95.
21 (*a*) L. Wang, Y. Z. Han, X. Feng, J. W. Zhou, P. F Qi and B. Wang, *Coord. Chem. Rev.*, 2016, **307**, 361–381; (*b*) L. Wang, X. Feng, L. Ren, Q. Piao, J. Zhong, Y. Wang, H. Li, Y. Chen and B. Wang, *J. Am. Chem. Soc.*, 2015, **137**, 4920–4923.
22 Q. Lai, Y. Zhao, Y. Liang, J. He and J. Chen, *Adv. Funct. Mater.*, 2016, DOI: 10.1002/adfm.201603607.
23 C. Liu, J. Wang, J. Li, J. Liu, C. Wang, X. Sun, J. Shen, W. Han and L. Wang, *J. Mater. Chem. A*, 2016, DOI: 10.1039/C6TA09193H.
24 Y. H. Lee, C. Z. Chang, S. L. Yau, L. J. Fan, Y. W. Yang, L. Y. O. Yang and K. Itaya, *J. Am. Chem. Soc.*, 2009, **131**, 6468–6474.
25 R. R. Salunkhe, C. Young, J. Tang, T. Takei, Y. Ide, N. Kobayashi and Y. Yamauchi, *Chem. Commun.*, 2016, **52**, 4764–4767.
26 M. Ramirez and D. D. L. Chung, *Carbon*, 2016, **110**, 8–16.
27 (*a*) J. H. Chen, W. Z. Li, D. Z. Wang, S. X. Yang, J. G. Wen and Z. F. Ren, *Carbon*, 2002, **40**, 1193–1197; (*b*) S. W. Lee, B. S. Kim, S. Chen, Y. S. Horn and P. T. Hammond, *J. Am. Chem. Soc.*, 2009, **131**, 671–679.
28 D. Y. Lee, D. V. Shinde, E. K. Kim, W. Lee, I. W. Oh, N. K. Shrestha, J. K. Lee and S. H. Han, *Microporous Mesoporous Mater.*, 2013, **171**, 53–57.
29 W. Meng, W. Chen, L. Zhao, Y. Huang, M. Zhu, Y. Huang, Y. Fu, F. Geng, J. Yu, X. Chen and C. Zhi, *Nano Energy*, 2014, **8**, 133–140.
30 C. Liu, J. Wang, J. Li, X. Hu, P. Lin, J. Shen, X. Sun, W. Han and L. Wang, *J. Mater. Chem. A*, 2016, **4**, 11916–11923.
31 Y. M. Chen, L. Yu and X. W. Lou, *Angew. Chem., Int. Ed.*, 2016, **55**, 5990–5993.
32 M. J. Shi, L. P. Zhao, X. F. Song, J. Liu, P. Zhang and L. Gao, *ACS Appl. Mater. Interfaces*, 2016, **8**, 32460–32467.

